A Methodology for Estimating the Parameters of a Gamma Raindrop Size Distribution Model from Polarimetric Radar Data: Application to a Squall-Line Event from the TRMM/Brazil Campaign

V. N. BRINGI, GWO-JONG HUANG, AND V. CHANDRASEKAR

Colorado State University, Fort Collins, Colorado

E. GORGUCCI

Istituto di Fisica dell'Atmosfera (CNR), Rome, Italy

(Manuscript received 25 June 2001, in final form 22 October 2001)

ABSTRACT

A methodology is proposed for estimating the parameters of a gamma raindrop size distribution model from radar measurements of Z_h, Z_{dr}, and K_{dp} at S band. Previously developed algorithms by Gorgucci et al. are extended to cover low rain-rate events where both Z_{dr} and K_{dp} are noisy. Polarimetric data from the S-band Dual-Polarization Doppler Radar (S-Pol) during the Tropical Rainfall Measuring Mission (TRMM)/Brazil campaign are analyzed; specifically, the gamma parameters are retrieved for samples of convective and trailing stratiform rain during the 15 February 1999 squall-line event. Histograms of N_w and D_o are retrieved from radar for each rain type and compared with related statistics reported in the literature. The functional behavior of N_w and D_o versus rain rate retrieved from radar is compared against samples of 2D-video and RD-69 disdrometer data obtained during the campaign. The time variation of N_w, D_o, and μ averaged over a 5 km $\times$ 5 km area (within which a network of gauges and a profiler were situated) is shown to illustrate temporal changes associated with the gamma parameters as the squall line passed over the network. The gauge-derived areal rainfall over the network is compared against radar using the areal Φ_{dp} method, and the concept of an effective slope of a linear axis ratio versus diameter model is shown to significantly reduce the bias in radar-derived rainfall accumulation.

1. Introduction

A long-standing goal in polarimetric radar has been the retrieval of the raindrop size distribution using measurements of reflectivity (Z_h), differential reflectivity (Z_{dr}), and specific differential phase (K_{dp}). Early studies focused on the estimation of D_o (the median volume diameter) or D_m (the mass-weighted mean diameter) using Z_{dr} measurements alone (Seliga and Bringi 1976; Goddard and Cherry 1984; Aydin et al. 1987; Bringi et al. 1998). The functional relation between D_o and Z_{dr} is known to be dependent on the mean axis ratio versus drop diameter relation, which can deviate from the equilibrium relation due to drop oscillations [e.g., Andsager et al. (1999); see also the summary in Pruppacher and Klett (1997) and numerous reference therein]. The same is also true for the functional relation between K_{dp} and rain rate. While the combined use of K_{dp} and Z_{dr} tends to mitigate somewhat the effects of drop oscillations on the estimation of rain rate (see Bringi and Chandrasekar 2001, chapter 7), a more satisfactory approach has been formulated in a series of papers by Gorgucci et al. (2000, 2001, 2002). The essential concept is related to the fact that drop oscillations and drop canting tend to bias the axis ratio toward sphericity, but this is generally nonlinear with respect to drop diameter. However, it is possible to define an equivalent linear model for the mean axis ratio versus D relation using an effective slope (β_{eff}), which can be estimated from radar measurements of Z_h, Z_{dr}, and K_{dp} and subsequently used in the estimation of the raindrop size distribution parameters. A background section is included that provides more detail on this concept.

At low rain rates, such as in stratiform rain, the polarimetric measurements of Z_{dr} and K_{dp} tend to be very noisy, unless the data are substantially averaged in space. In such cases, the effective β method cannot be applied, and in this paper a method is proposed for retrieval of the drop size distribution (DSD) parameters in the gamma model. The normalized gamma DSD with parameters (D_o, N_w, and μ) is suitable for inverting the radar measurements. The normalization procedure

Corresponding author address: Dr. V. N. Bringi, Electrical and Computer Engineering, Colorado State University, Fort Collins, CO 80523.
E-mail: bringi@engr.colostate.edu

(which defines the normalized intercept parameter N_w) can be found in Willis (1984) or Testud et al. (2001).

In this paper S-band Dual-Polarization Doppler Radar (S-Pol) data collected during the Tropical Rainfall Measuring Mission (TRMM)/Brazil field campaign are analyzed to provide the statistics of D_o and N_w in samples of convective and stratiform rain during a squall-line episode on 15 February 1999 that lasted several hours. The behavior of D_o and N_w versus rain rate is also analyzed and compared with 2D video (Joanneum Research) and RD-69 (Disdromet, Ltd.) disdrometer measurements of samples of convective and stratiform rain obtained during the field campaign. The hypothesis that the use of β_{eff} in polarimetric rain-rate algorithms will reduce the bias in cumulative rainfall is tested by comparing with a network of gauges for the 15 February case.

2. Background

The radar measurement set of reflectivity at horizontal polarization (Z_h), differential reflectivity (Z_{dr}), and specific differential phase (K_{dp}) can in the Rayleigh scattering limit be related to the microphysics of raindrops. Specifically, the Z_h is related to the sixth moment of the DSD, Z_{dr} is related to the reflectivity-weighted mean axis ratio, and K_{dp} is related to the product of the water content and the deviation of the mass-weighted mean axis ratio from unity (Jameson 1983, 1985). If a model relating the axis ratio (r) of oriented oblate raindrops versus the equivolumic spherical diameter (D) is selected, then Z_{dr} can be related to the reflectivity-weighted mean diameter of the DSD, while K_{dp} can be related to the product of W and D_m (the mass-weighted mean diameter of the DSD). Generally, the linear fit to the wind-tunnel data of Pruppacher and Beard (1970), $r = 1.03 - 0.062D$ (with D in mm), or the numerical equilibrium shape model of Beard and Chuang (1987) has been used. If the DSD is modeled as a normalized gamma form (Willis 1984; Testud et al. 2001),

$$N(D) = N_w f(\mu)\left(\frac{D}{D_o}\right)^{\mu} e^{-(3.67+\mu)(D/D_o)} \tag{1a}$$

with

$$f(\mu) = \frac{6}{(3.67)^4}\frac{(3.67 + \mu)^{\mu+4}}{\Gamma(\mu + 4)} \tag{1b}$$

where N_w is the normalized intercept parameter of an equivalent exponential DSD that has the same water content and median volume diameter (D_o) as the gamma DSD, then it follows that $Z_h = N_w F_1(\mu) D_o^7$, $Z_{\text{dr}} = F_2(\mu, D_o)$, while $K_{\text{dp}} = N_w F_3(\mu, D_o)$ where F represents a functional form. Thus, in principle, estimates of D_o, N_w, and μ (and W or rain rate R) can be obtained from the radar measurement set of (Z_h, Z_{dr}, and K_{dp}). Note that D_o and D_m are related by $D_o/D_m = (3.67 + \mu)/(4 + \mu)$ (Ulbrich and Atlas 1998).

The effects of raindrop shape oscillations (either due to resonance maintained by vortex shedding or due to collisions) and raindrop canting (due to turbulence) will bias the retrieval of the gamma DSD parameters under the above model assumptions (e.g., see Bringi and Chandrasekar 2001, chapter 7 and references therein). Both drop oscillations and canting angle distributions tend on average to drive the effective axis ratio toward sphericity relative to equilibrium axis ratios and perfect orientation. The rain microphysics model can be improved by accounting for drop oscillations using the axis ratio versus D fit proposed by Andsager et al. (1999) and by using a Gaussian canting angle distribution with a mean of 0° and a standard deviation (σ) in the range 5°–10° (Bringi and Chandrasekar 2001). For example, if the axis ratio versus D relation is assumed to be linear with a slope of (β), $r = 1 - \beta D$, then K_{dp} is modified as (see Bringi and Chandrasekar 2001)

$$K_{\text{dp}} = \beta N_w F_3(\mu, D_o) \exp(-2\sigma^2) \tag{2a}$$

$$= \beta_{\text{eff}} N_w F_3(\mu, D_o). \tag{2b}$$

Gorgucci et al. (2000) recognized that drop canting and oscillations could be incorporated into an ''effective'' slope parameter (β_{eff}) and proceeded to develop an algorithm to estimate β_{eff} from the radar measurement set (Z_h, Z_{dr}, K_{dp}). It is important to recognize that even if drop axis ratio is in fact a nonlinear function of D, it is possible to define an equivalent linear model with a slope of β_{eff} such that it results in the same K_{dp} (for a given value of the product WD_o) as the nonlinear form. In subsequent articles, Gorgucci et al. (2001, 2002) developed algorithms (see summary in the appendix) for retrieving rain rate (R) as well as D_o, N_w, and μ using β_{eff} in combination with the measurement pair (Z_h, Z_{dr}). They show via comparisons with disdrometer DSD measurements that D_o and N_w can be retrieved with excellent accuracy (ranging from 4%–8% for D_o and $\log_{10}N_w$). Simulations were also used to study the effects of radar measurement error in the retrieval of D_o and N_w, and it was found that the accuracy was still quite good (ranging from 5%–20% for D_o and $\log_{10}N_w$) and, more importantly, the estimates were nearly unbiased. The μ estimator was found to be less accurate, though it may be possible to distinguish between certain ranges of μ, for example, $-1 \leq \mu \leq 2$ versus $\mu > 5$, which may be sufficient in practice.

The concept of an ''effective'' slope (β_{eff}) of the mean axis ratio versus D relation is an important one since drop oscillations or canting are likely to be different in, for example, tropical rain versus rain in the midlatitudes. Oscillations/canting may be suppressed when rain is formed via melting of graupel or tiny hail as compared with warm rain formation. Gorgucci et al. (2001) applied the β_{eff} concept to an unusual tropical-like flash flood–producing storm in Colorado and showed that rain-rate estimators based on β_{eff}, Z_h, and Z_{dr} resulted in better agreement with gauge data as compared with

the standard $R(K_{dp})$ algorithm (see, also, Petersen et al. 1999). May et al. (1999) also found that use of the Pruppacher and Beard equilibrium shape model (β fixed at 0.062 mm^{-1}) resulted in a systematic underestimate in rainfall when using $R(K_{dp})$, as compared with a dense gauge network in the Tropics, and attributed this bias to drop oscillations causing an upward shift in mean axis ratio (toward sphericity). More recently, Fulton et al. (1999) have suggested an empirical adjustment to the $R(K_{dp})$ algorithm using a multiplicative bias correction factor, $B(\langle Z_{dr}\rangle)$, which they found reduced the temporal bias in rain accumulation. This correction factor, though empirical, tends to account for the tendency of drop oscillations/canting to cause an upward shift in mean axis ratio. Thus, there appears to be sufficient evidence to warrant further application of the effective β concept to retrieve D_o, N_w, and μ, as well as rain rate, and this is the principal objective of this paper.

Since β_{eff} is estimated from the measurement set (Z_h, Z_{dr}, K_{dp}), and K_{dp} at long wavelengths (such as S band) is known to be very noisy at low rain rates, it follows that the retrieval of the DSD parameters is only practical when the rain rate is sufficiently high (typical threshold of $Z_h \geq 35$ dBZ). At low rain rates, such as in stratiform rain, the Z_{dr} also tends to be noisy so that a large areal average is necessary to reduce the measurement fluctuations. Thus, it is necessary to extend the retrieval of DSD parameters (D_o and N_w) at low rain rates ($Z_h <$ 35 dBZ), at which K_{dp} and at times Z_{dr} are generally too noisy to be useful; this is another goal of this paper. Finally, the last goal is to compare radar-derived rain rates against a network of gauges to illustrate the application of β_{eff} in reducing the rainfall accumulation bias. The data sources used are the S-Pol radar, 2D-video and RD-69 disdrometers, and a network of gauges deployed for the TRMM/Brazil field campaign[1] held in 1999 in Amazonia. Data from a squall line on 15 February 1999 are used for analysis.

3. Data analysis methods

a. S-Pol radar

The S-Pol radar is a dual-polarized radar operating at a frequency near 2.8 GHz (S band). It uses a mechanical polarization switch and two separate receivers to measure the polarimetric covariance matrix (Randall et al. 1997). The datastream used here consists of Z_h, Z_{dr}, and Φ_{dp} (differential propagation phase), which are available every 150 m in range. For each beam of data, a ''good'' data mask is generated based on the standard deviation of Φ_{dp} over 10 consecutive gates ($<10°$), the copolar correlation coefficient ($\rho_{co} \geq 0.9$), and the signal-to-noise ratio (SNR $\geq$ 3 dB). These thresholds tend to eliminate nearly all nonmeteorological echoes. The Φ_{dp} range profile is filtered according to Hubbert and Bringi (1995). Once the filtered Φ_{dp} range profile is obtained, K_{dp} is calculated based on the slope of a least squares fit line to the filtered Φ_{dp} profile in an adaptive manner (30 consecutive range samples are used in the linear fit for $Z_h <$ 35 dBZ; 20 for 35 $< Z_h \leq$ 45 dBZ; and 10 for $Z_h >$ 45 dBZ). The Z_h is corrected for attenuation using the algorithm of Testud et al. (2000) adapted for S band, while Z_{dr} is corrected for differential attenuation using a self-consistent, constraint-based algorithm described by Bringi et al. (2001b). Corrections are significant only when $\Phi_{dp} \geq 50°$. The corrected Z_h and Z_{dr} range profiles are averaged in range using uniform block averaging for the different Z_h ranges described earlier. The effective β is calculated based on the averaged Z_h, Z_{dr}, and K_{dp} data, and $D_o(\beta_{eff}, Z_h, Z_{dr})$, $N_w(\beta_{eff}, Z_h, Z_{dr})$, and $R(\beta_{eff}, Z_h, Z_{dr})$ are calculated using the algorithms given in the appendix. The threshold for computing β_{eff} is based on $Z_h \geq 35$ dBZ, $Z_{dr} \geq 0.2$ dB, and $K_{dp} \geq 0.3°$ km^{-1}.

When the $Z_h <$ 35 dBZ, which occurs for light rainfall (e.g., stratiform rain), a different retrieval method, which is based on disdrometer measurements, is proposed for D_o and N_w.

b. Disdrometer

A 2D-video disdrometer (Schönhuber et al. 1995) and a RD-69 disdrometer (Joss and Waldvogel 1967) were available during the TRMM/Brazil field campaign. These two instruments were sited close to each other and near the National Oceanic and Atmospheric Administration (NOAA) profilers. (For a description of the 2D-video instrument refer to the Web site http://www.disdrometer.at.) Because of technical difficulties the 2D-video disdrometer was not operating continuously through the field campaign. However, it is believed that representative samples of DSD measurements were made in convective rain (164 2-min-averaged DSD samples) and stratiform rain (49 2-min-averaged samples). The stratification of rain types was based on manual examination of profiler reflectivity/velocity images, for example, absence or presence of a ''bright band.'' RD-69 disdrometer data were available more or less throughout the field campaign. In this study, the RD-69 DSD data were selected during those times when the 2D-video was operational. The 2D-video disdrometer has a large sample volume relative to the RD-69 disdrometer (Tokay et al. 1999). Intercomparisons between these two instruments are available in Tokay et al. (1999) and Williams et al. (2000). The latter study demonstrates the underestimation of small drops ($<$1.5 mm) by the RD-69 at higher rain rates (reflectivity $\geq$ 40 dBZ), which causes the mass-weighted mean diameter (D_m) and R to be biased low relative to the 2D-video disdrometer. At low rain rates the D_m and R from both instruments are in very good agreement. The underestimation of small drops by the RD-69 also tends

[1] A detailed description of the instrumentation can be found online at http://radarmet.atmos.colostate.edu/lab_trmm.

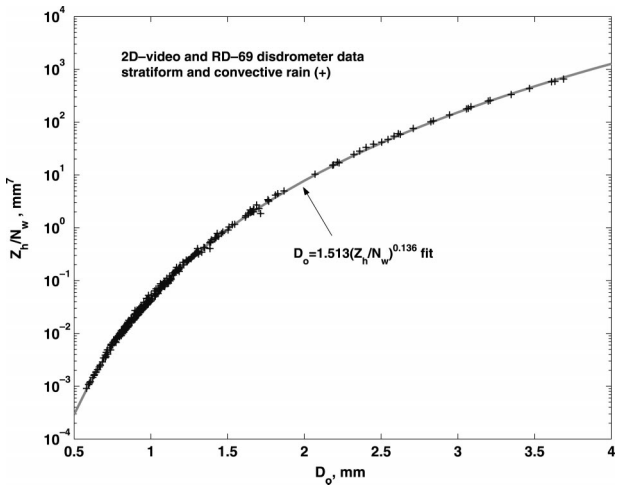

FIG. 1. Scatterplot of Z_h/N_w vs D_o based on gamma fits to 2D-video (in convective and stratiform rain) and RD-69 (in stratiform rain) disdrometer data obtained during the TRMM/Brazil field campaign. Each data point (+) refers to a 2-min-averaged DSD to which a gamma DSD is fitted. There are 164 2-min samples of convective rain from the 2D-video and 152 2-min samples of stratiform rain from the 2D-video and RD-69. The power law fit is also shown.

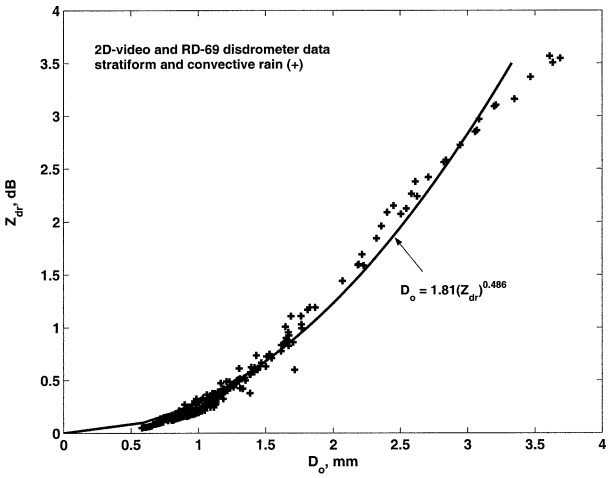

FIG. 2. As in Fig. 1, except Z_{dr} vs D_o. Power law fit is based on rain rates exceeding 2 mm h^{-1}.

to increase the convex shape of the DSD (i.e., higher μ values). The 2D-video measurements of small drops are affected by windy conditions (Nespor et al. 2000), because small drops ''can get caught in a vortex that develops over the inlet. Some of them end up being counted more than once as they cross the sensing area while others are carried away and not counted at all. Also, the spatial distribution of the drops passing across the sensing area is distorted by the wind'' (Nespor et al. 2000). To ensure the quality of the 2D-video data, the spatial distribution of drops across the sensor area (available during real-time operations and during post-processing) was carefully examined, and no evidence was found of any distortion due to wind in the events analyzed. In addition, a terminal velocity filter was applied to the data; that is, any drop whose terminal velocity exceeded a prespecified ''band'' around the theoretical value [$v(D) = 9.65 - 10.3 \exp(-0.6D)$, m s^{-1}; Atlas et al. (1973)] was rejected.

In this study, only the 2D-video data in convective rain were used. In stratiform rain both the 2D-video and RD-69 data have been used, to increase the number of samples. For each 2-min-averaged DSD, the parameters of a normalized gamma DSD (N_w, D_o, μ) were obtained using a method previously described in the appendix of Bringi et al. (2001a). In short, the water content (W, in g m^{-3}) and the mass-weighted mean diameter (D_m, in mm) are calculated first, after which the N_w is obtained as $N_w = (256/\pi)(1000W/D_m^4)$, in mm^{-1} m^{-3}. The normalized DSD is constructed as $N(x) = N(D/D_m)/N_w$, and μ is estimated by minimizing the absolute deviation between $\log[N(x)]$ and $\log\{f(\mu)x^\mu \exp[-(4 + \mu)x]\}$. This method separates the estimation of μ, the DSD shape, from the normalizing parameters D_m and N_w and is philosophically similar to the method of Sempere-Torres et al. (1994). Other methods are available to estimate (N_w, D_m, μ) (see, e.g., Willis 1984; Ulbrich and Atlas 1998). For each triplet of gamma DSD parameters, the reflectivity at horizontal polarization (Z_h), Z_{dr}, and K_{dp} are computed at 2.8 GHz, assuming (i) mean axis ratio fit recommended by Andsager et al. (1999) for $1 \le D \le 4$ mm, which accounts for transverse drop oscillations, and the Beard and Chuang (1987) equilibrium axis ratio fit for $D < 1$ and $D > 4$ mm; (ii) Gaussian canting angle distribution with mean of 0° and $\sigma = 10°$; and (iii) size integration up to $D_{max} = 2.5D_m$. As shown in the appendix, when the simulated Z_h, Z_{dr}, and K_{dp} are used in (A4) the resultant β_{model} is not constant but varies with D_o in a regular manner (see A5). These model assumptions appear to be valid for tropical rain (Bringi et al. 2001a). Note, however, that this model will generally be used for retrieval of N_w and D_o for light rain rates ($Z_h < 35$ dBZ).

Figure 1 shows a plot of Z_h/N_w versus D_o where the data points are from the gamma fit to 2D-video data in convective and stratiform rain, and from the RD-69 in stratiform rain. Also shown is the power law fit $D_o = 1.513(Z_h/N_w)^{0.136}$, where the exponent is close to the theoretically expected value of 1/7 = 0.143 expected for Rayleigh scattering by spherical drops. The exponent is slightly smaller because the drops are oblate. It is important to note that the exponent is accurately determined from the plot of (Z_h/N_w) versus D_o as compared to the determination of both the multiplicative coefficient and the exponent from a plot of Z_h versus D_o, which displays much more scatter. The disdrometer analysis in Fig. 1 shows that

$$D_o = 1.513(N_w)^{-0.136} Z_h^{0.136} = \gamma Z_h^{0.136} \qquad (3)$$

(note that Z_h here is in mm^6 m^{-3}). This fit will be used to retrieve D_o from Z_h for light rain rates when the measurement of Z_{dr} falls below the threshold of 0.2 dB.

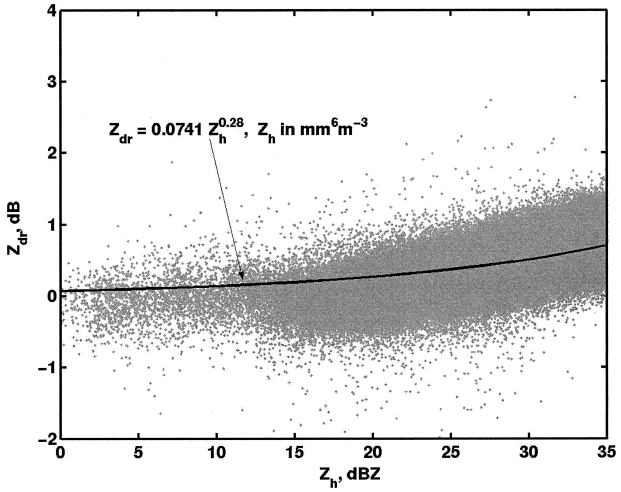

FIG. 3. S-Pol radar measurements of Z_{dr} vs Z_h from stratiform rain on 15 Feb 1999, together with a mean power law fit.

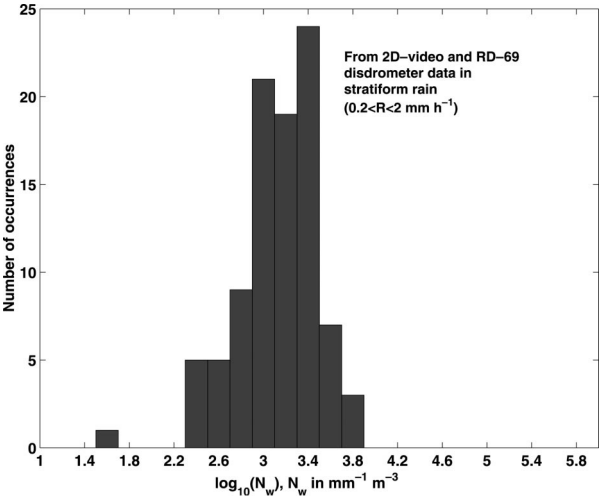

FIG. 4. Histogram of $\log_{10}N_w$ in stratiform rain from gamma fits to 2-min-averaged DSD data collected by the 2D-video and RD-69 during the TRMM/Brazil campaign.

However, the estimate of γ will be obtained in a manner to be described later [see (6b)].

Figure 2 shows a plot of Z_{dr} versus D_o. The power law fit to these data result in,

$$D_o = 1.81(Z_{dr})^{0.486}. \quad (4)$$

For radar measurements with $Z_h < 35$ dBZ and $Z_{dr} \geq 0.2$ dB, the D_o is retrieved using (4), and N_w is retrieved from (3), which is expressed as

$$N_w = \frac{21Z_h}{D_o^{7.353}}; \quad \text{mm}^{-1}\ \text{m}^{-3}, \quad (5)$$

where Z_h is in mm^6 m^{-3}.

For radar measurements with $Z_h < 35$ dBZ and $Z_{dr} < 0.2$ dB the following method is proposed. Using (3) and (4), D_o can be eliminated to obtain a relation between Z_h and Z_{dr} of the form $Z_{dr} = \alpha Z_h^{\delta}$ where δ is the ratio of the exponents in (3) and (4) given by $\delta = 0.136/0.486 \approx 0.28$. The coefficient α can be determined, in practice, from all radar measurements of Z_{dr} with corresponding $Z_h < 35$ dBZ. The estimate $\hat{\alpha}$ is easily determined as $\hat{\alpha} = \langle Z_{dr}\rangle/\langle Z_h^{0.37}\rangle$ where angle brackets denote a spatial average; note that Z_{dr} is in dB and Z_h in mm^6 m^{-3}. Figure 3 shows a scatterplot of Z_{dr} versus Z_h for radar data in stratiform rain from 15 February 1999 as well as the power law fit with $\hat{\alpha} = 0.0741$ (this value is close to that obtained from disdrometer analysis, 0.0842). The essential hypothesis is that even though Z_{dr} measurements are noisy at low reflectivities and tend on average to near 0 dB at very light rain rates, scattering simulations based on disdrometer DSD samples and a rain model with β_{model} as in (A5) indicate that the mean relation should follow a power law of form $Z_{dr} = \alpha Z_h^{0.28}$. Thus, a method exists for retrieving D_o, even if the individual resolution volumes have $Z_{dr} < 0.2$ dB (the prespecified threshold). First, $\hat{\alpha}$ is determined from the data, which includes all Z_{dr} values with $Z_h < 35$ dBZ (the lower bound of Z_h is set to 0 dBZ here). Next, (4) is used with $Z_{dr} = \hat{\alpha}(Z_h)^{0.28}$ to arrive at

$$D_o = 1.81(\hat{\alpha})^{0.468}(Z_h)^{0.136}; \quad \text{mm} \quad (6a)$$

$$= \hat{\gamma}(Z_h)^{0.136} \quad (6b)$$

where $\hat{\gamma} = 1.81(\hat{\alpha})^{0.486}$. Subsequently, N_w is obtained from (3) as

$$N_w = (1.513/\hat{\gamma})^{7.35}; \quad \text{mm}^{-1}\ \text{m}^{-3} \quad (7)$$

Note that this retrieval N_w can be interpreted as an estimate of the expected value of N_w, since $\hat{\alpha}$ is an estimate of the expected value of α. For example, the expected value of N_w for the stratiform rain data in Fig. 3 is 2920 mm^{-1} m^{-3}. If σ_α is the standard deviation of $\hat{\alpha}$ then a range of N_w values is to be expected, and as a first approximation N_w may be assumed to be uniformly distributed between $[N_{w1}, N_{w2}]$ where the lower and upper values correspond to using $\hat{\alpha} + \sigma_\alpha/2$ and $\hat{\alpha} - \sigma_\alpha/2$ in (7) and noting that $\hat{\gamma} = 1.81(\hat{\alpha})^{0.486}$. Analysis of a large number of volumes of radar measurements of (Z_h, Z_{dr}) pairs in both convective and stratiform rain types on 15 February 1999 suggests that σ_α is around 0.015, which puts the 1/2 standard deviation bounds of N_w in the range 2100–4300 mm^{-1} m^{-3}. To demonstrate that these assumptions are reasonable, Fig. 4 shows a histogram of $\log_{10}(N_w)$ from the combined set of 2D-video and RD-69 data in stratiform rain (composite from different days during TRMM/Brazil). Note from Fig. 4 that the N_w values in stratiform rain range between 250 and 6000 mm^{-1} m^{-3} with the mode being 2500 mm^{-1} m^{-3}.

To summarize the retrieval of D_o and N_w from radar measurements, if the measurement set (Z_h, Z_{dr}, K_{dp}) exceeds the thresholds of 35 dBZ, 0.2 dB, and 0.3° km^{-1}, respectively, then the algorithms using β_{eff} as described in the appendix are used. If $Z_h < 35$ dBZ and $Z_{dr} \geq 0.2$ dB, then D_o and N_w are retrieved via (4) and (5), re-

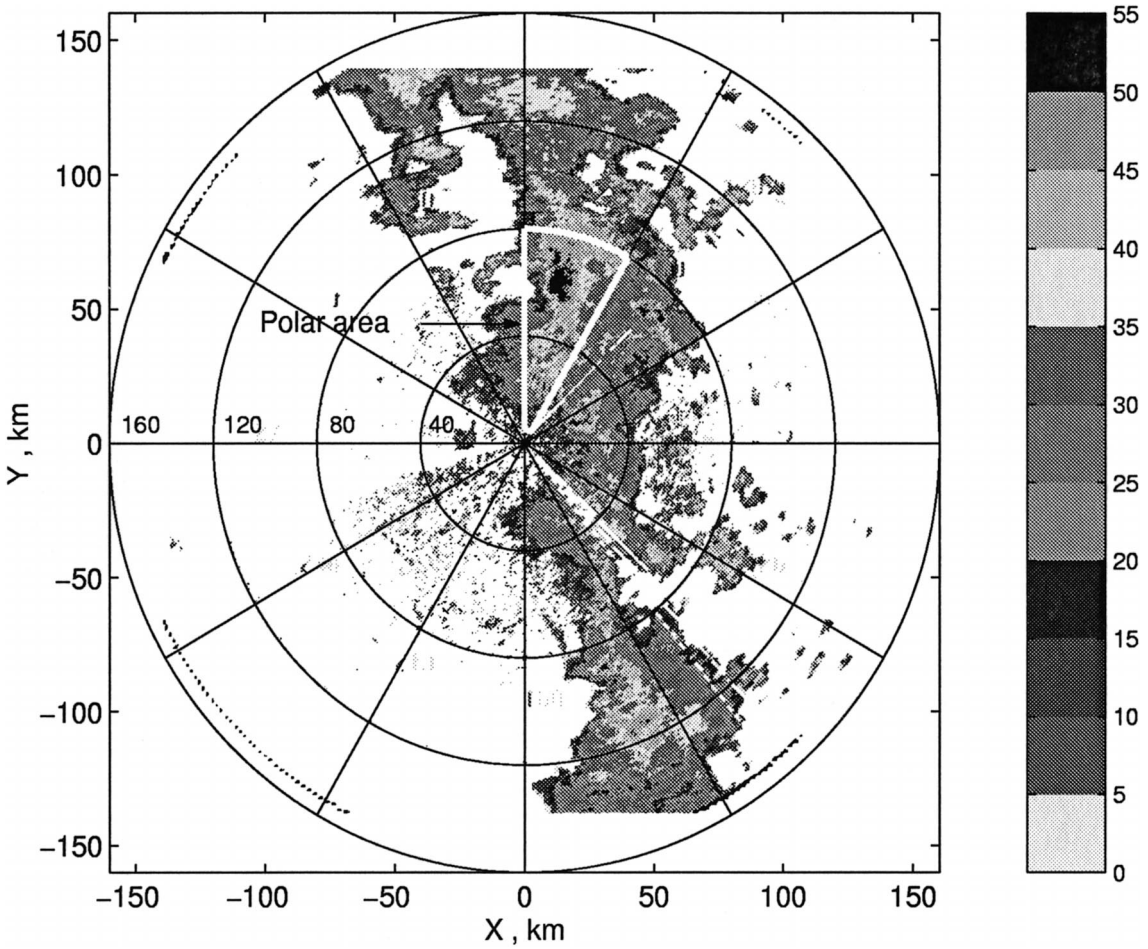

FIG. 5. PPI of reflectivity at 0350 UTC of the 15 Feb squall line. The polar area marked illustrates the region of convective rain selected for the radar-based retrieval of N_w and D_o.

spectively. If $Z_h < 35$ dBZ and $Z_{dr} < 0.2$ dB, then D_o is retrieved using (6) and N_w using (7), with the added provision of distributing N_w uniformly in a prescribed range. The DSD shape parameter (μ) is not retrieved in this case and is set to zero. The rain rate is derived assuming $\mu = 0$ (exponential shape) and using the retrieved N_w and D_o and the terminal velocity relation $v = 3.78D^{0.67}$ from Atlas and Ulbrich (1977).

4. Results from 15 February 1999

a. Statistics of D_o and N_w

On 15 February 1999 of the TRMM/Brazil field campaign,[2] a squall line formed to the east of the S-Pol radar and moved westward, crossing the measurement area over a period of 4 hours (0300–0800 UTC; all times henceforth will be UTC). The squall line was well organized as a north–south line during the early phase (0300–0400) but became disorganized past 0430 with a number of strong cells embedded within a large area of weak echo. Past 0700, there was a transition from convective to primarily stratiform rain. Figure 5 shows the squall line as a PPI of Z_h (in dBZ) at 0350. The polar area marked in the figure refers to the area where retrieval of D_o and N_w was performed, and is presumed to be representative of strong convective rain within the squall line. Figure 6 shows histograms of radar-derived (a) D_o and (b) $\log_{10}N_w$ for rain rates < 10 (mm h^{-1}), while similar histograms for $R \geq 10$ (mm h^{-1}) are shown in Fig. 7. Figure 6a shows that the spread in D_o is relatively large at the lower rain rates compared to Fig. 7a, while the modal N_w in Fig. 6b is near 1000 mm^{-1} m^{-3} as compared to 20 000 mm^{-1} m^{-3} in Fig. 7b. The lower concentration of larger drops for $R < 10$ mm h^{-1} likely represents nonequilibrium distributions similar to data from positive Z_{dr} columns (Caylor and Illingworth 1987; Bringi et al. 1991), whereas the D_o, N_w histograms for $R > 10$ mm h^{-1} reflect data from more mature rainshafts (narrower spread in D_o). Figure 8 shows D_o and N_w versus rain rate; also plotted are

[2] S-Pol radar images for this day at 10-min intervals can be viewed online at http://www.atd.ucar.edu/rsf/TRMM-LBA/quicklook/990215.

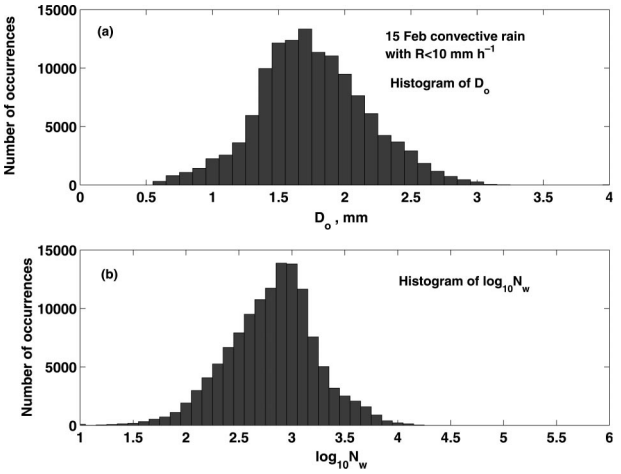

FIG. 6. Histogram of (a) D_o and (b) $\log_{10}N_w$ based on radar retrievals for convective rain with $R < 10$ (mm h^{-1}) from the polar area marked in Fig. 5.

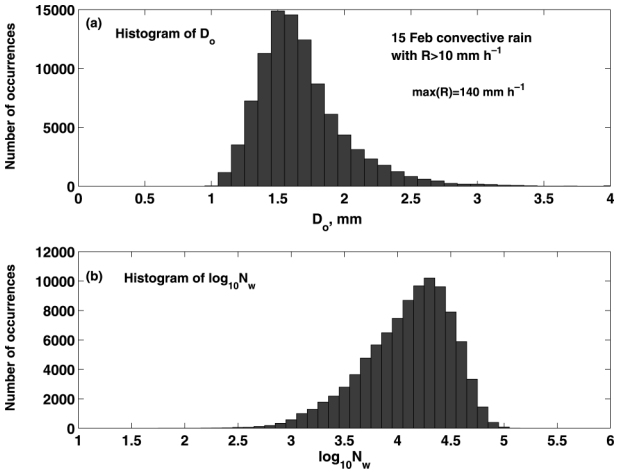

FIG. 7. As in Fig. 6, except for convective rain with $R > 10$ (mm h^{-1}).

data from the 2D-video disdrometer in convective rain from all times during the TRMM/Brazil project during which it was operational. The radar retrievals do not show any obvious functional dependence of either D_o or N_w on rain rate, except possibly for D_o at the very lowest rates. The disdrometer D_o does show an increasing trend with R (for $R \leq 5$ mm h^{-1}) in agreement with the radar-retrieved D_o. There is general agreement between the disdrometer and radar retrievals with regard to the spread of D_o and N_w, even though the radar retrievals are from a specific convective area of the 15 February squall line, whereas the 2D-video data are from a small sample of different types of convective rain in the same region.

Figure 9 shows the histogram of D_o and $\log_{10}N_w$ from an area of stratiform rain at 0756 on 15 February. Vertical sections of Z_h and Z_{dr} (not shown here) indicated a ''brightband'' feature, and there was no convection that could be interpreted from the images. The spread of D_o around its mode is now significantly smaller as compared to Fig. 6a. The spread of N_w around its mode (modal value $\approx$ 2000 mm^{-1} m^{-3}) is also smaller in stratiform rain compared with Fig. 6b. The D_o and N_w histograms in stratiform rain are generally comparable to those derived from airborne imaging probes by Testud et al. (2001) for stratiform rain during Tropical Ocean Global Atmosphere Coupled Ocean–Atmosphere Response Experiment (TOGA COARE) (see their Fig. 3). In particular, their mean and standard deviation of D_o (1.21 and 0.28 mm, respectively) can be compared with Fig. 9a (corresponding values of 1.34 and 0.24 mm). Similarly, for the mean and standard deviation of $\log_{10}N_w$, Testud et al. (2001) obtained 3.48 and 0.5 versus 3.31 and 0.28 from Fig. 9b. It is, in fact, remarkable that these statistics for a sample of stratiform rain from Brazil derived by polarimetric radar generally agree with a more complete ensemble of stratiform rain from TOGA COARE, despite large sample volume differences. Of course, it is well known that convective rain characteristics over land and ocean are very different, and the histograms for convective rain in Fig. 6 do not agree with the Testud et al. (2001) analysis of convective rain from TOGA COARE for $R < 10$ mm h^{-1}. However, the statistics for $R > 30$ mm h^{-1} are in good agreement, as summarized in Tables 1 and 2.

One possible reason for the general agreement of the statistics in stratiform rain from these two climatic regimes may be due to similarity in the dominant microphysical processes leading to rain formation (i.e., rain formed from melting aggregates). As for the agreement in convective rain in the higher rain-rate regime ($R >$ 30 mm h^{-1}), it may be that the microphysical processes leading to an equilibrium-type DSD are similar in the two regimes (e.g., Hu and Srivastava 1995).

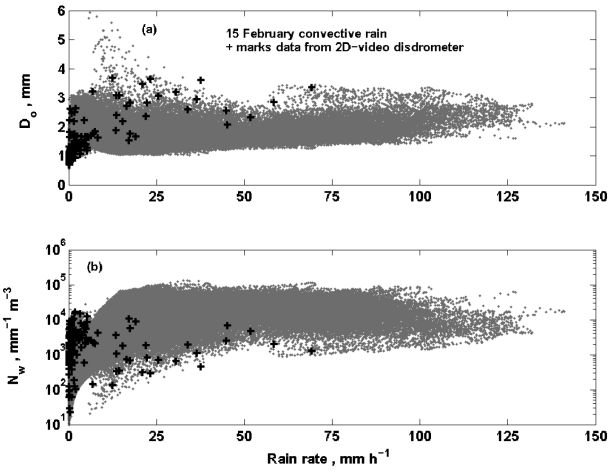

FIG. 8. Scatterplot of (a) D_o vs R and (b) N_w vs R for convective rain from the polar area marked in Fig. 5. Overlaid are data from the 2D-video disdrometer in convective rain collected during the TRMM/Brazil campaign (164 2-min-averaged DSD samples).

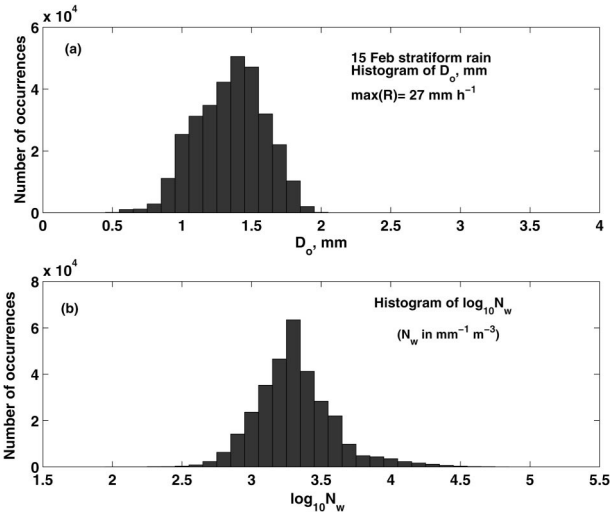

FIG. 9. As in Fig. 6, except for stratiform rain at 0756 UTC 15 Feb 1999. Data are from a different polar area (not shown).

The biggest difference in Tables 1 and 2 is related to the case of convective rain with $R < 10$ mm h^{-1}, which from the radar perspective is characteristic of a lower concentration of relatively larger drops as compared with the Testud et al. (2001) results and with the stratiform rain results. This is not surprising, given that warm rain processes as well as drop sorting (Carbone and Nelson 1978; Atlas et al. 1999) are likely to be dominant in the updraft area of the convective portion of the squall line leading to nonequilibrium-type DSD spectra, similar to those found in positive Z_{dr} columns. Stronger updraft over land versus ocean could be one reason why the statistics of D_o and N_w in the low rain-rate category ($R < 10$ mm h^{-1}) from the radar retrievals are so different from the convective TOGA COARE statistics derived by Testud et al. (2001).

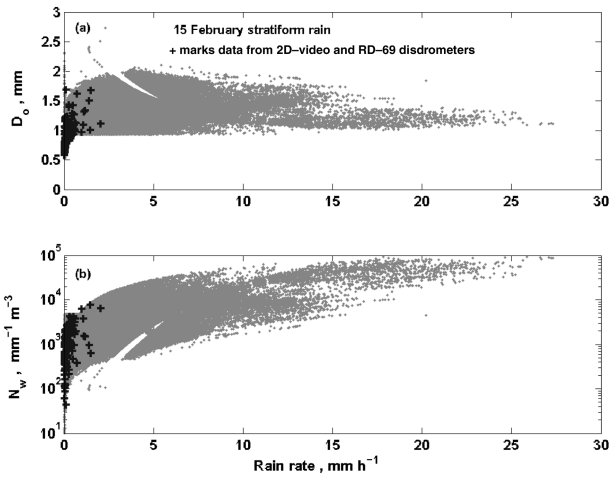

FIG. 10. As in Fig. 8, except data from stratiform rain. Overlaid are data from 2D-video and RD-69 disdrometers in stratiform rain collected during TRMM/Brazil (152 2-min-averaged DSD samples).

TABLE 1. Statistics of D_o.

Rain type	Mean and (std dev) of D_o from S-Pol radar	Mean and (std dev) of D_o from Testud et al. (2001)
Convective, with $R > 30$ mm h^{-1}	1.75 mm (0.34)	1.66 mm (0.33)
Stratiform	1.34 mm (0.24)	1.21 mm (0.26)
Convective, with $R < 10$ mm h^{-1}	1.76 mm (0.42)	1.13 mm (0.27)

Figure 10 shows radar-retrieved D_o and N_w versus R for stratiform rain; also plotted are the 2D-video and RD-69 data from samples of stratiform rain during times when the 2D-video was operational. Good agreement may be noted with regard to the range of D_o and N_w predicted by radar and disdrometer at very low rain rates ($R < 2$ mm h^{-1}). There appears to be a functional relation between D_o and R at these low rain rates but for $R > 5$ mm h^{-1}, if there is any correlation between D_o and R and between N_w and R, it is very weak.

b. Time profile of DSD parameters

Because the 15 February squall line was long lived, it is possible to show how the DSD parameters and rain rate changed with time over a 3-h period as the squall line moved over one of the gauge networks. Figure 11a shows the location of the gauges relative to the S-Pol radar as well as a polar area surrounding the gauges. The various gauge rain rates were averaged over 2-min intervals and represent the mean areal R versus time over the polar area. The DSD parameters were also averaged over the polar area and represent areal average quantities. While the gauge locations were not uniformly distributed over the selected polar area, the storm system was large enough that a good estimate of mean areal rain rate is believed to have been obtained.

Figure 11b shows the time–height profile of reflectivity from the 915-MHz vertically pointing profiler. The profiler and the 2D-video and RD-69 disdrometers were located at the Ji Parana airport (see Fig. 11a). Three convective cells may be noted in Fig. 11b at 4.75, 5.75, and 6.5 h (times are in fractions of an hour, UTC).

Figures 12a and 12b show the time profile of areally averaged D_o, N_w, and μ, as well as the mean areal R from

TABLE 2. Statistics of $\log_{10}N_w$.

Rain type	Mean and (std dev) of $\log_{10}N_w$ from S-Pol radar	Mean and (std dev) of $\log_{10}N_w$ from Testud et al. (2001)
Convective, with $R > 30$ mm h^{-1}	4.22 (0.34)	4.20 (0.33)
Stratiform	3.31 (0.28)	3.48 (0.52)
Convective, with $R < 10$ mm h^{-1}	2.81 (0.42)	4.00 (0.52)

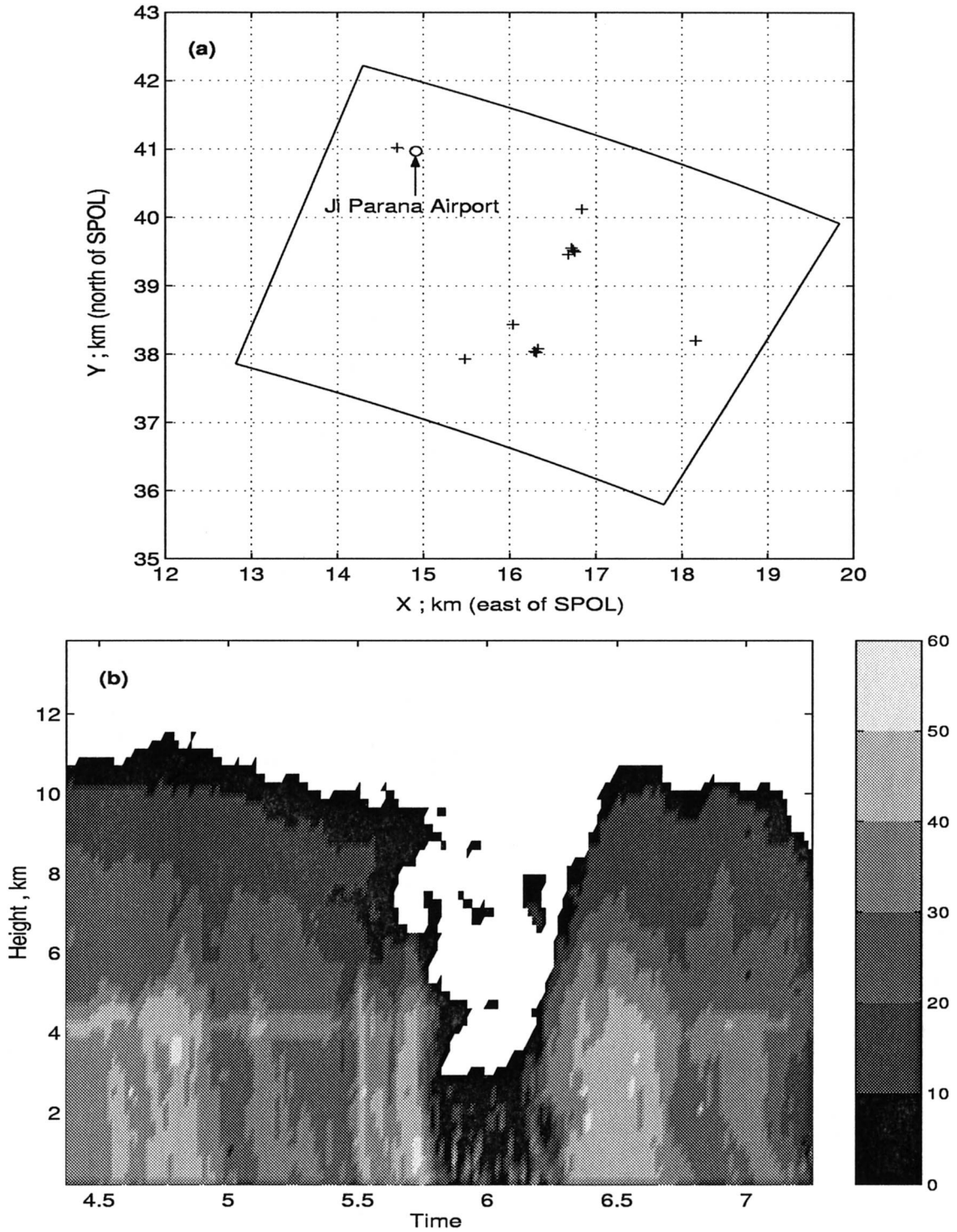

FIG. 11. (a) Polar area shows the gauge network. The 2D-video and RD-69 disdrometers and the NOAA profiler were located at the Ji Parana airport. (b) Time–height profile of reflectivity from the NOAA 915-MHz vertically pointing Doppler radar (or profiler).

the gauge network. Three convective rain cells can be identified in the time profile (abscissa is time in fractions of an hour; e.g., 4.5 means 0430 UTC) with D_o's in the range 1.4–1.5 mm, N_w around 15 000 $\text{mm}^{-1}\ \text{m}^{-3}$, and μ around 3–5 near the rain cell peaks. In the stratiform rain between the rain cell peaks, the D_o's are around 0.7 mm, N_w is in the range 1500–2500 $\text{mm}^{-1}\ \text{m}^{-3}$, and μ is around 1–2 (e.g., centered around times at 0515 UTC, or 5.25 and 7.125 h). Vertical profiles of the reflectivity from the NOAA profiler[3] showed a bright band between the rain cell peaks (see Fig. 11b). It is emphasized that the radar-derived D_o, N_w, and μ values are areally averaged (over the polar area shown in Fig. 11a).

To illustrate the use of the effective β in reducing the bias in rainfall accumulation, the areal R (or AR) is derived using differential propagation phase (Φ_{dp}) using the algorithm proposed and evaluated by Bringi et al. (2001a):

$$\text{AR} = \frac{c}{2}\int_{\theta_1}^{\theta_2}\left\{[r_2\Phi_{\text{dp}}(r_2,\,\theta) - r_1\Phi_{\text{dp}}(r_1,\,\theta)] - \int_{r_1}^{r_2}\Phi_{\text{dp}}(r,\,\theta)\,dr\right\}d\theta \tag{8}$$

In the above, r_1, r_2, θ_1, and θ_2 describe the limits of the polar area (see Fig. 11). For a given beam with constant azimuth angle θ, AR depends on the boundary values of Φ_{dp} as well as the area under the Φ_{dp} range profile. As the azimuthal angle changes from θ_1 to θ_2, an areal sweep of Φ_{dp} over the rain region occurs naturally, performing a spatial integration of the rainfall. A linear relation between R and K_{dp} of the form $R = cK_{\text{dp}}$ is assumed to be valid locally to derive (8). Since the actual relation is nonlinear, a piecewise linear approximation is proposed, as shown in Fig. 13. The rain model used in the simulations is described in relation to (A5) in the appendix. Because a sufficiently large database of disdrometer data was not available from TRMM/Brazil, the simulations in Fig. 13 are based on an entire season of rain DSD measurements made with the RD-69 disdrometer near Darwin, Australia. When AR is divided by the polar area it will be termed the mean areal rain rate ($\overline{R}$). The multiplicative coefficient c in (8) is selected based on the average K_{dp} along a specific beam according to the piecewise linear fit in Fig. 13. This approach avoids the necessity of assuming a priori that K_{dp} is constant along the various beams (Ryzhkov et al. 2000). The cumulative rainfall using the fixed rain model with β_{model} as in (A5) results in a bias (overestimate) of around 20% when compared with the gauge network accumulation, as illustrated in Fig. 14. Simulations performed by Gorgucci et al. (2001) show that the $R(K_{\text{dp}})$ estimator varies as $R = c'K_{\text{dp}}\beta_{\text{eff}}^{-1.5}$. To correct for changing β_{eff} relative to β_{model} in (A5), the modal value of β_{eff} is first computed over the polar area in Fig. 11a from radar measurements of Z_h, Z_{dr}, and K_{dp} (see appendix), and this is done as a function of time. Next, the modal value of ξ_{dr}(Z_{dr} in linear scale) is used to calculate β_{model} using (A5). The areal rain rate is then adjusted by the factor $(\beta_{\text{model}}/\beta_{\text{eff}})^{1.5}$. During stratiform rain periods, the Z_h, K_{dp}, and Z_{dr} generally fall below the threshold required for the calculation of β_{eff} and, thus, no adjustment is done during these periods. Figure 14 also shows the rain accumulation after correcting for β_{eff}, and the accumulation bias has now been reduced to $<10\%$. The main advantage of using the β_{eff}-based correction is that the effects of drop oscillations and/or drop canting is implicity accounted for in the rain-rate algorithm. One simply starts with theoretical rain model or disdrometer DSD data for the regime (or, similar to the regime under consideration) to arrive at a first approximation for the R–K_{dp} relation, and then the radar data are used to correct for deviations of β_{eff} from the assumed model value [β_{model} in (A5)] in a relatively straightforward manner. The results shown here suggest that the use of disdrometer data from Darwin to arrive at the piecewise linear fit in Fig. 13 is valid for setting the initial R–K_{dp} relation, and, in fact, demonstrates the power of the effective β method. Such an approach avoids the use of empirical-based methods suggested by Fulton et al. (1999).

5. Summary and conclusions

A method is proposed for retrieving the parameters D_o and N_w of a normalized gamma DSD using radar measurements of Z_h, Z_{dr}, and K_{dp} at S band (frequency near 3 GHz). The algorithms based on the effective β concept derived by Gorgucci et al. (2001, 2002) have been extended to low rain rates where both K_{dp} and Z_{dr} tend to be noisy and preclude an accurate estimate of β_{eff}. Disdrometer data and scattering simulations are used to retrieve the D_o and N_w at low rain rates. Thus, the combined method retrieves D_o and N_w over the full range of rain rates detectable by radar.

Statistics of D_o and N_w in the form of histograms were presented for convective and stratiform samples of rain data in one squall-line event from the TRMM/Brazil field campaign using the S-Pol radar. The mean and standard deviation of D_o and $\log_{10}N_w$ in stratiform rain compared favorably with similar statistics presented by Testud et al. (2001) based on airborne measurements during TOGA COARE. In convective rain, the statistics

[3] Vertical profiles of reflectivity from the NOAA profiler can be viewed online at http://www.al.noaa.gov/WWWHD/pubdocs/TropDyn/trmmlba/al915/bra_b00_105_1999046.gif.

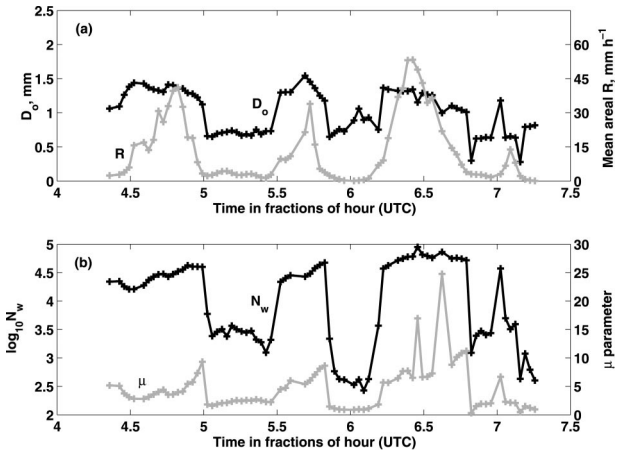

FIG. 12. Time variation of (a) D_o and mean areal R from gauges, and (b) $\log_{10}N_w$ and μ. The DSD parameters are areally averaged over the polar area shown in Fig. 11a.

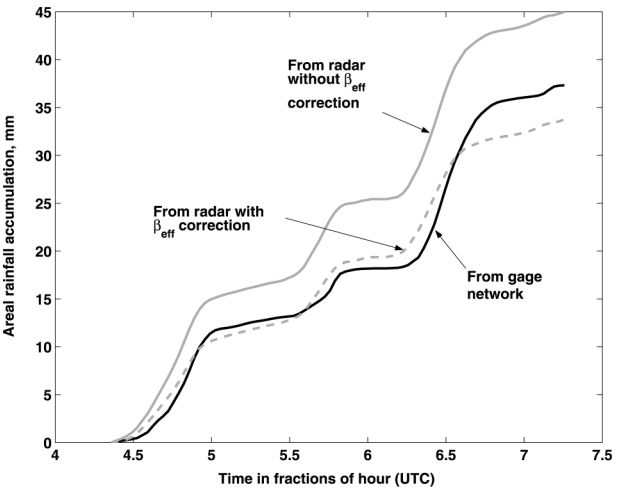

FIG. 14. Areal rainfall accumulation over the polar area in Fig. 11a from radar (using the areal Φ_{dp} method) and the gauge network vs time. Illustrates the use of β_{eff} in reducing the bias in radar rainfall accumulation to less than 10%.

for the higher rain-rate category ($R \geq 30$ mm h^{-1}) also agreed with Testud et al. (2001). This agreement, which is based on a very limited sample of radar data, may suggest that the dominant microphysical processes are similar, for example, melting of snow to form stratiform rain or the tendency to equilibrium-like distributions in heavier convective rain. The statistics were, however, quite different in lighter convective rain ($R < 10$ mm h^{-1}) with much larger mean D_o over land as compared with TOGA COARE and, correspondingly, much lower values of N_w. It will be necessary to repeat the radar retrievals before firmer conclusions can be made, but the methodology proposed herein is an important step and makes it possible now to proceed with such studies in different climatic regimes where high quality dual-polarized radar data are available: for example, Darwin, Australia; the South China Sea Monsoon Experiment (SCSMEX); the Texas–Florida Underflight Experiment (TEFLUN-B) in Florida; and the Severe Thunderstorm and Electrification Project (STEPS) in Colorado.

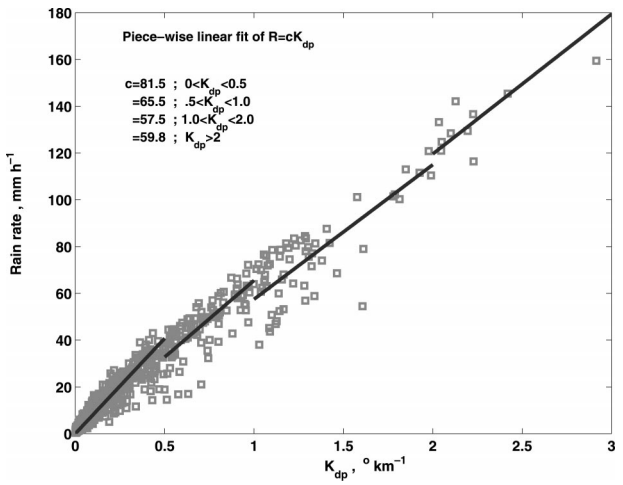

FIG. 13. The piecewise linear fit, $R = cK_{dp}$, needed for the areal rain-rate algorithm using Φ_{dp}. The data points are from scattering simulations based on a large database of RD-69 disdrometer DSDs from Darwin, Australia (over 2000 2-min DSD samples) in a variety of rain types.

The functional behavior of the retrieved D_o and N_w with rain rate in samples of stratiform and convective rain was studied and compared with samples of 2D-video and RD-69 disdrometer measurements in similar rain types during TRMM/Brazil. The agreement, in terms of the range of D_o and N_w values, was good. At low rain rates ($R < 5$ mm h^{-1}), there appeared to be a correlation between D_o and R. Weak correlation was found between D_o and R or N_w and R in both the radar retrievals as well as the disdrometer data for $R > 5$ mm h^{-1}. Generally, these results are supportive of the Testud et al. (2001) analysis of airborne DSD data from TOGA COARE.

The 15 February squall-line event analyzed in this paper also shows how the β_{eff} estimate was used to remove the bias in accumulated rainfall when using the areal rain-rate estimator based on differential propagation phase via comparison with a gauge network deployed over a 5 km $\times$ 5 km area. The time profile of areally averaged D_o, N_w, and μ was determined as three consecutive convective rain cells moved over the gauge network area with periods of stratiform rain in between. Within the convective rain cells the D_o values ranged from 1.4 to 1.5 mm, with N_w around 15 000 mm^{-1} m^{-3} and μ around 3–5. In stratiform rain the corresponding ranges were 0.6–0.7 mm, N_w around 1500–2500 mm^{-1} m^{-3}, and μ around 1–2. These ranges are in general agreement with past studies (e.g., Cifelli et al. 2000; Tokay and Short 1996). Future research will be directed toward comparison with DSD retrievals from profilers (e.g., Williams et al. 2000).

The success of the proposed methodology in provid-

ing for unbiased estimates of D_o, N_w, or μ relies on accurate calibration of the radar; specifically, the accuracy in Z_h should be 1 dB or better and for Z_{dr} it should be 0.1 dB or better. Also, to retrieve the gamma DSD parameters at low rain rates, disdrometer DSD samples in convective and stratiform rain should be available for setting algorithm coefficients/exponents, specifically in the power laws $D_o = aZ_{dr}^b$ and $Z_h/N_w = cD_o^{7.35}$. Correction for attenuation effects will be important at C band and higher frequencies. Even at S band, correction of Z_h and Z_{dr} data is important when the differential propagation phase becomes large ($\geq 50°$). Techniques to correct for attenuation are now available (Testud et al. 2000; Bringi et al. 2001b; Smyth and Illingworth 1998).

Acknowledgments. This research was supported by the NASA/TRMM Grants NAG5-7717 and NAG5-7876. VNB also acknowledges support from the National Science Foundation via ATM-9612519 for analysis of the 2D-video disdrometer data. Drs. John Hubbert, John Beaver, and Steve Bolen of CSU were instrumental in supporting the operation of the NASA 2D-video disdrometer during TRMM/Brazil. Dr. C. R. Williams provided the profiler data used to construct Fig. 11.

APPENDIX

Retrieval Algorithm for D_o, N_w, and μ

The method of retrieving D_o, N_w, and μ from Z_h, Z_{dr}, and K_{dp} is summarized here from Gorgucci et al. (2001, 2002). A gamma DSD model is assumed with the following ranges for the parameters:

$$0.5 \leq D_o \leq 3.5 \text{ mm} \tag{A1}$$

$$3 \leq \log_{10} N_w \leq 5 \tag{A2}$$

$$-1 < \mu \leq 5 \tag{A3}$$

with the additional constraint that $R < 300$ mm h^{-1}. The parameters D_o, $\log_{10} N_w$, and μ are varied uniformly over their respective ranges to form a large table of D_o, N_w, and μ. Scattering calculations are performed at 2.8 GHz over a range of β_{eff}, and nonlinear regression is used to develop an algorithm for β (henceforth, the subscript ''eff'' will be dropped) in terms of Z_h, Z_{dr}, and K_{dp}:

$$\beta = 2.08 Z_h^{-0.365} K_{dp}^{0.38} \xi_{dr}^{0.965} \tag{A4}$$

where Z_h is in mm^6 m^{-3}, K_{dp} in $°$ km^{-1}, and ξ_{dr} is the differential reflectivity expressed as a ratio ($Z_{dr} = 10 \log_{10} \xi_{dr}$).

Simulations using gamma fits to measured drop size distributions (see section 3b) and scattering calculations at 2.8 GHz of Z_h, Z_{dr}, and K_{dp}, assuming (i) mean axis ratio versus D fit of Andsager et al. (1999) for $1 \leq D \leq 4$ mm and Beard and Chuang (1987) for $D < 1$ and $D > 4$ mm, (ii) Gaussian canting angle distribution with mean 0° and $\sigma = 10°$, and (iii) size integration up to $D_{max} = 2.5 D_m$, show that β_{model} using (A4) is generally clustered around 0.045–0.0475 mm^{-1} but is a nonlinear function of D_o (or equivalently ξ_{dr}). A nonlinear fit to the simulations yields

$$\beta_{model} = 0.0049(\xi_{dr})^2 - 0.0043(\xi_{dr}) + 0.0433; \quad \xi_{dr} > 1. \tag{A5}$$

The median volume diameter is then derived as

$$D_o = aZ_h^b (\xi_{dr})^c \tag{A6}$$

where,

$$a = 0.56, \tag{A7}$$

$$b = 0.064, \tag{A8}$$

$$c = 0.024\beta^{-1.42}. \tag{A9}$$

The N_w is derived as

$$\log_{10} N_w = aZ_h^b (\xi_{dr})^c \tag{A10}$$

where now

$$a = 3.29, \tag{A11}$$

$$b = 0.058, \tag{A12}$$

$$c = -0.023\beta^{-1.389}, \tag{A13}$$

and μ is derived as

$$\mu = \frac{aD_o^b}{(\xi_{dr} - 1)} - c(\xi_{dr})^d \tag{A14}$$

where

$$a = 200\beta^{1.89}, \tag{A15}$$

$$b = 2.23\beta^{0.039}, \tag{A16}$$

$$c = 3.16\beta^{-0.046}, \tag{A17}$$

$$d = 0.374\beta^{-0.355}. \tag{A18}$$

The rain rate is derived as

$$R = 0.105\beta^{0.865} Z_h^{0.93} (\xi_{dr})^c \tag{A19}$$

where

$$c = -0.585\beta^{-0.703}. \tag{A20}$$

In this paper, the thresholds used are $Z_h \geq 35$ dBZ, $Z_{dr} \geq 0.2$ dB, and $K_{dp} \geq 0.3°$ km^{-1} for retrieval of D_o, N_w, μ, and R using the above algorithms.

REFERENCES

Andsager, K., K. V. Beard, and N. F. Laird, 1999: Laboratory measurements of axis ratios for large raindrops. *J. Atmos. Sci.,* **56,** 2673–2683.

Atlas, D., and C. W. Ulbrich, 1977: Path- and area-integrated rainfall measurement by microwave attenuation in the 1–3 cm band. *J. Appl. Meteor.*, **16,** 1322–1331.

——, R. C. Srivastava, and R. S. Sekhon, 1973: Doppler radar char-

acteristics of precipitation at vertical incidence. *Rev. Geophys. Space Phys.,* **2,** 1–35.

——, C. W. Ulbrich, F. D. Marks Jr., E. Amitai, and C. R. Williams, 1999: Systematic variation of drop size and radar–rainfall relations. *J. Geophys. Res.,* **104** (D6), 6155–6169.

Aydin, K., H. Direskeneli, and T. A. Seliga, 1987: Dual-polarization radar estimation of rainfall parameters compared with ground-based disdrometer measurements: October 29, 1982, central Illinois experiment. *IEEE Trans. Geosci. Remote Sens.,* **GE-25,** 834–844.

Beard, K. V., and C. Chuang, 1987: A new model for the equilibrium shape of raindrops. *J. Atmos. Sci.,* **44,** 1509–1524.

Bringi, V. N., and V. Chandrasekar, 2001: *Polarimetric Doppler Weather Radar: Principles and Applications.* Cambridge University Press, 648 pp.

——, D. A. Burrows, and S. M. Menon, 1991: Multiparameter radar and aircraft study of raindrop spectral evolution in warm-based clouds. *J. Appl. Meteor.,* **30,** 853–880.

——, V. Chandrasekar, and R. Xiao, 1998: Raindrop axis ratios and size distributions in Florida rainshafts: An assessment of multiparameter radar algorithms. *IEEE Trans. Geosci. Remote Sens.,* **36,** 703–715.

——, G. Huang, V. Chandrasekar, and T. D. Keenan, 2001a: An areal rainfall estimator using differential propagation phase: Evaluation using a C-band radar and a dense gauge network in the Tropics. *J. Atmos. Oceanic Technol.,* **18,** 1810–1818.

——, T. D. Keenan, and V. Chandrasekar, 2001b: Correcting C-band radar reflectivity and differential reflectivity data for rain attenuation: A self-consistent method with constraints. *IEEE Trans. Geosci. Remote Sens.,* **39,** 1906–1915.

Carbone, R. E., and L. D. Nelson, 1978: The evolution of raindrop spectra in warm-based convective storms as observed and numerically modeled. *J. Atmos. Sci.,* **35,** 2302–2314.

Caylor, I. J., and A. J. Illingworth, 1987: Radar observations and modeling of warm rain initiation. *Quart. J. Roy. Meteor. Soc.,* **113,** 1171–1191.

Cifelli, R., C. R. Williams, D. K. Rajopadhyaya, S. K. Avery, K. S. Gage, and P. T. May, 2000: Drop-size distribution characteristics in tropical mesoscale convective systems. *J. Appl. Meteor.,* **39,** 760–777.

Fulton, R. A., A. V. Ryzhkov, and D. S. Zrnić, 1999: Areal rainfall estimation using conventional and polarimetric radar methods. Preprints, *29th Conf. on Radar Meteorlogy,* Montreal, QC, Canada, Amer. Meteor. Soc., 293–296.

Goddard, J. W. F., and S. M. Cherry, 1984: The ability of dual-polarization radar (copolar linear) to predict rainfall rate and microwave attenuation. *Radio Sci.,* **19,** 201–208.

Gorgucci, E., G. Scarchilli, V. Chandrasekar, and V. N. Bringi, 2000: Measurement of mean raindrop shape from polarimetric radar observations. *J. Atmos. Sci.,* **57,** 3406–3413.

——, G. Scarchilli, V. Chandrasekar, and V. N. Bringi, 2001: Rainfall estimation from polarimetric radar measurements: Composite algorithms immune to variability in raindrop shape–size relation. *J. Atmos. Oceanic Technol.,* **18,** 1773–1786.

——, V. Chandrasekar, V. N. Bringi, and G. Scarchilli, 2002: Estimation of raindrop size distribution parameters from polarimetric radar measurements. *J. Atmos. Sci.,* in press.

Hu, Z., and R. C. Srivastava, 1995: Evolution of raindrop size distribution by coalescence, breakup, and evaporation: Theory and observations. *J. Atmos. Sci.,* **52,** 1781–1783.

Hubbert, J., and V. N. Bringi, 1995: An iterative filtering technique for the analysis of copolar differential phase and dual-frequency radar measurements. *J. Atmos. Oceanic Technol.,* **12,** 643–648.

Jameson, A. R., 1983: Microphysical interpretation of multi-parameter radar measurements in rain. Part I: Interpretation of polarization measurements and estimation of raindrop shapes. *J. Atmos. Sci.,* **40,** 1792–1802.

——, 1985: Microphysical interpretation of multi-parameter radar measurements in rain. Part III: Interpretation and measurement of propagation differential phase shift between orthogonal linear polarizations. *J. Atmos. Sci.,* **42,** 607–614.

Joss, J., and A. Waldvogel, 1967: A raindrop spectrograph with automatic analysis. *Pure Appl. Geophys.,* **68,** 240–246.

May, P. T., T. D. Keenan, D. S. Zrnić, L. D. Carey, and S. A. Rutledge, 1999: Polarimetric radar measurements of tropical rain at a 5-cm wavelength. *J. Appl. Meteor.,* **38,** 750–765.

Nespor, V., W. F. Krajewski, and A. Kruger, 2000: Wind-induced error of raindrop size distribution measurement using a two-dimensional video disdrometer. *J. Atmos. Oceanic Technol.,* **17,** 1483–1492.

Petersen, W. A., and Coauthors, 1999: Mesoscale and radar observations of the Fort Collins flash flood of 28 July 1997. *Bull. Amer. Meteor. Soc.,* **80,** 191–216.

Pruppacher, H. R., and K. V. Beard, 1970: A wind tunnel investigation of the internal circulation and shape of water drops falling at terminal velocity in air. *Quart. J. Roy. Meteor. Soc.,* **96,** 247–256.

——, and J. D. Klett, 1997: *Microphysics of Clouds and Precipitation.* 2d ed. Kluwer Academic, 955 pp.

Randall, M., J. Lutz, and J. Fox, 1997: S-POL's high isolation mechanical polarization switch. Preprints, *28th Conf. on Radar Meteorology,* Austin, TX, Amer. Meteor. Soc., 252–253.

Ryzhkov, A., D. S. Zrnić, and R. Fulton, 2000: Areal rainfall estimates using differential phase. *J. Appl. Meteor.,* **39,** 263–268.

Schönhuber, M., H. E. Urban, J. P. V. Baptista, W. L. Randeu, and W. Riedler, 1995: Weather radar versus 2D-video disdrometer data. Preprints, *Third Int. Symp. on Hydrological Applications of Weather Radars,* Sao Paulo, Brazil, 351–360.

Seliga, T. A., and V. N. Bringi, 1976: Potential use of radar differential reflectivity measurements at orthogonal polarizations for measuring precipitation. *J. Appl. Meteor.,* **15,** 69–76.

Sempere-Torres, D., J. M. Porrà, and J. D. Creutin, 1994: A general formulation for raindrop size distribution. *J. Appl. Meteor.,* **33,** 1494–1502.

Smyth, T. J., and A. J. Illingworth, 1998: Correction for attenuation of radar reflectivity using polarization data. *Quart. J. Roy. Meteor. Soc.,* **124,** 2393–2415.

Testud, J., E. Le Bouar, E. Obligis, and M. Ali-Mehenni, 2000: The rain profiling algorithm applied to polarimetric weather radar. *J. Atmos. Oceanic Technol.,* **17,** 322–356.

——, S. Oury, P. Amayenc, and R. A. Black, 2001: The concept of ''normalized'' distributions to describe raindrop spectra: A tool for cloud physics and cloud remote sensing. *J. Appl. Meteor.,* **40,** 1118–1140.

Tokay, A., and D. A. Short, 1996: Evidence from tropical raindrop spectra of the origin of rain from stratiform and convective clouds. *J. Appl. Meteor.,* **35,** 355–371.

——, and O. W. Thiele, A. Kruger, and W. F. Krajewski, 1999: New measurements of drop size distribution and its impact in radar rainfall retrievals. Preprints, *29th Conf. on Radar Meteorology,* Montreal, QC, Canada, Amer. Meteor. Soc., 659–662.

Ulbrich, C. W., and D. Atlas, 1998: Rainfall microphysics and radar properties: Analysis methods for drop size spectra. *J. Appl. Meteor.,* **37,** 912–923.

Williams, C. R., A. Kruger, K. S. Gage, A. Tokay, R. Cifelli, W. F. Krajewski, and C. Kummerow, 2000: Comparison of simultaneous raindrop size distributions estimated from two surface disdrometers and a UHF profiler. *Geophys. Res. Lett.,* **27,** 1763–1766.

Willis, P. T., 1984: Functional fits to some observed drop size distributions and parameterization of rain. *J. Atmos. Sci.,* **41,** 1648–1661.